THE ASTRONOMICAL JOURNAL, 115:2579–2586, 1998 June

WIDE FIELD PLANETARY CAMERA 2 OBSERVATIONS OF THE BROWN DWARF GLIESE 229B: OPTICAL COLORS AND ORBITAL MOTION

D. A. GOLIMOWSKI,[1] C. J. BURROWS,[2] S. R. KULKARNI,[3] B. R. OPPENHEIMER,[3] AND R. A. BRUKARDT[1]

Received 1997 December 11; revised 1998 February 17

ABSTRACT

Three-epoch observations of the M1 V–plus–brown dwarf system Gliese 229AB using the *Hubble Space Telescope*'s Wide Field Planetary Camera 2 (WFPC2) are reported. Relative astrometric measurements spanning 1 year confirm the common proper motion of the pair and reveal the first evidence of orbital motion. The radial and azimuthal components of Gl 229B's relative motion are $-0\farcs087$ and $+0\farcs049$, respectively, indicating an elliptical orbit rather than an inclined circular orbit. The absolute WFPC2 magnitudes of Gl 229B are $M_{1042} = 16.37$, $M_{814} = 20.76$, and $M_{675} = 24.60$, assuming a distance of 5.774 pc. The detection of Gl 229B through the F675W bandpass is the first reported at *R*-band wavelengths. The measured flux through F1042M ($\lambda_c \approx 1$ μm) is well matched by the latest models of dust-free brown dwarf photospheres by Tsuji et al. These models severely overestimate the broadband fluxes shortward of 0.8 μm, however, which indicates that a strong source of optical continuum opacity exists in the photosphere of Gl 229B. A search for fainter companions to Gl 229A in the Planetary Camera was negative to limiting absolute magnitudes of $M_{1042} \approx 19$ and $M_{814} \approx 24.5$ beyond 7″ of Gl 229A. Nondetection limits for the Wide Field Cameras are 1.5 mag greater than those for the Planetary Camera.

Key words: binaries: close — stars: individual (Gliese 229B) — stars: low-mass, brown dwarfs

1. INTRODUCTION

Brown dwarfs are compact objects with masses below the minimum mass required for stable hydrogen burning. Nakajima et al. (1995, hereafter N95) reported the first unambiguous discovery of a cool brown dwarf, Gliese 229B, from a coronagraphic survey of nearby stars with ages of $\sim$1 Gyr. N95 identified Gl 229B as a common proper motion companion of the nearby star Gl 229 (=HD 42581 = LHS 1827; $V = 8.14$, spectral type M1 V; hereafter Gl 229A). The near-infrared spectrum of Gl 229B shows strong absorption by CH_4 and H_2O (Oppenheimer et al. 1995; Geballe et al. 1996) and resembles the reflection spectra of the giant outer planets in our solar system.

Using observed broadband fluxes from 0.8 to 10.5 μm and a distance to Gl 229A of 5.7 pc, Matthews et al. (1996, hereafter M96) derived a bolometric luminosity of $\sim 6.4 \times 10^{-6}$ $L_\odot$ for Gl 229B, well below the minimum luminosity for hydrogen-burning stars ($L_{\rm min} \approx 10^{-4}$ $L_\odot$; Burrows & Liebert 1993). Assuming a radius for Gl 229B equal to that of Jupiter (Burrows & Liebert 1993), M96 obtained $T_{\rm eff} \approx 900$ K. At this effective temperature, the brown dwarf's atmosphere is expected to be composed primarily of H_2, H_2O, CH_4, and N_2 (Tsuji & Ohnaka 1995; Fegley & Lodders 1996). Thus, the strong CH_4 absorption first noted by Oppenheimer et al. (1995) supports the $T_{\rm eff}$ derived by M96. Spectral models of cool brown dwarfs predict that Gl 229B has a dust-free photosphere (Tsuji et al. 1996) and an effective temperature of 900–1000 K (Allard et al. 1996; Marley et al. 1996). This temperature range implies a mass of $\sim$0.03–0.055 $M_\odot$ for a likely age of 1–5 Gyr (Allard et al. 1996; Marley et al. 1996). Optical spectra of Gl 229B indicate an absence of TiO and VO, commonly associated with metal-rich M dwarfs, suggesting that Ti and V have condensed and settled as dust in the lower atmosphere (Oppenheimer 1998; Schultz et al. 1998; Oppenheimer et al. 1998). Recent near-infrared spectra reveal CO in greater abundance than expected for equilibrium with CH_4 at $T_{\rm eff} \approx 900$ K, possibly because of convective mixing from warmer layers of the upper atmosphere (Noll, Geballe, & Marley 1997; Oppenheimer et al. 1998). Such mixing is observed in Jupiter's atmosphere (Noll et al. 1988) and may provide clues about the formation and internal structure of Gl 229B.

In this paper, we present the results of three-epoch observations of Gl 229B using the Wide Field Planetary Camera 2 (WFPC2) aboard the *Hubble Space Telescope* (*HST*). These observations comprise four *HST* orbits granted by the director of the Space Telescope Science Institute (STScI) from his discretionary observing time. Using the high astrometric accuracy of *HST*, we confirm that Gl 229AB is a common proper motion pair and report the first evidence of orbital motion. We also present optical broadband photometry of Gl 229B, including the first measurement in the *R* bandpass. Finally, we provide limits on the brightness of other possible companions located beyond 0″.25 from Gl 229A.

2. OBSERVATIONS AND DATA REDUCTION

Observations of Gl 229AB were performed on UT 1995 November 17, 1996 May 26, and 1996 November 11 using WFPC2. Gl 229A was acquired at the approximate center of the Planetary Camera (PC), providing a $33\farcs5 \times 33\farcs5$ field of view (FOV) centered on the star. Telescope roll angles of 328° (epochs 1 and 3) and 148° (epoch 2) were selected so that the position angle of Gl 229B (P.A. = 163°; N95) would not coincide with the diffraction spikes or the charge overflow from the saturated image of Gl 229A. Data from the three Wide Field Cameras (WFCs) were also obtained,

[1] Department of Physics and Astronomy, Johns Hopkins University, 3400 North Charles Street, Baltimore, MD 21218.
[2] Space Telescope Science Institute, 3700 San Martin Drive, Baltimore, MD 21218; and Astrophysics Division, Space Science Department, European Space Agency.
[3] Palomar Observatory, Mail Stop 105-24, California Institute of Technology, Pasadena, CA 91125.

providing partial coverage of the circumstellar field up to 2′ from Gl 229A.

First-epoch images were recorded through three broadband filters: F675W (WFPC2 *R*), F814W (WFPC2 *I*), and F1042M ($\lambda_c \approx 1$ μm) (Burrows et al. 1995). To guarantee accurate astrometry of Gl 229AB, unsaturated images of each component were obtained by recording sets of four short (1.6 s) and two long (300 s) exposures through F1042M. Between the exposures of each set, the pointing was offset in successive steps of 0.″2275 (5 PC pixels) along the rows and columns of the CCD. These offsets ensured that neither cosmic-ray events nor defective pixels would skew the image centroids. Similarly, two-exposure sets of 0.11, 5, and 400 s were recorded through F814W. These sets permitted inspection of the circumstellar field with varying sensitivity beyond 0.″25 from Gl 229A. One 500 s exposure through F675W was also obtained, completing the two-orbit time allocation. For the 0.11, 1.6, and 5 s exposures, a gain of 14 e^- DN^{-1} was used to minimize detector saturation by Gl 229A. For the longer exposures, a gain of 7 e^- DN^{-1} was used to enhance sensitivity to faint field sources. During the exposures longer than 1.6 s, the pixels in the PC's serial register were continually clocked to minimize the effect of charge overflow.

Second-epoch observations of Gl 229AB were conducted with the telescope rolled 180° from the first-epoch roll angle. Gl 229A was acquired $\sim 3''$ from the nominal first-epoch pointing. At this roll angle, the FOV of each WFC was diametrically opposite Gl 229A from its corresponding first-epoch FOV. Because of the asymmetric focal-plane configuration of the WFPC2 CCDs (Burrows et al. 1995), approximately 20% of the total WFC FOV was imaged in both the first and second epochs. Sets of two 1.6 s exposures and two 300 s exposures were recorded through F1042M, and two 400 s exposures were obtained with F814W. (The F814W exposures produced images of distant field stars needed for astrometric measurements of Gl 229AB.) As before, pointing offsets of 0.″2275 were performed along each CCD axis between the exposures of each set.

Third-epoch images were obtained with the telescope rolled at the same angle used during the first-epoch observations. Gl 229A was acquired $\sim 0.''4$ from the nominal first-epoch pointing. Although the sequence of exposures was intended to be the same as that used during the second epoch, a miscommunication during observation planning resulted in a sequence of exposures through F1042M identical to that used during the first epoch. No exposures through F814W were obtained. The consequences of this miscommunication are discussed in § 3.2.

The data were flux-calibrated using the Space Telescope Science Data Analysis System (STSDAS) software and the calibration reference files recommended by the *HST* data archive for each epoch. The images of each exposure set were shifted by 5 PC pixels in each axis to a common registration coinciding with the nominal telescope pointing. The shifted images then were combined to produce a single image devoid of cosmic-ray or "hot pixel" artifacts. The final images represented the average of their constituent exposures after rejection of pixel values at least 3 σ above the mean value at that location. For the single F675W image, artifacts were identified by visual inspection.

Subtraction of Gl 229A's point-spread function (PSF) from the vicinity of point sources in the PC field was performed using the NOAO IRAF task IMSURFIT. Bivariate Legendre polynomials were fitted to the PSF outside a circular aperture encompassing each source and lying within a 25×25 pixel subimage centered on that source. The fitted surfaces were then subtracted from the subimage, providing noiseless removal of the PSF. Image centers and fluxes of each source were determined by averaging individual measurements of each from the PSF-subtracted subimages created from polynomial fits of varying order.

The astrometric and photometric measurements for all sources in the WFPC2 FOV were obtained using conventional methods of aperture photometry. The image centers were determined using an image centroid algorithm in which only those pixels having intensities above the mean intensity of the photometry aperture were used (Da Costa 1992). The centroids were then transformed to distortion-free coordinates using the STSDAS task METRIC (Gilmozzi, Ewald, & Kinney 1995). The measured fluxes were converted to instrumental magnitudes by applying the aperture corrections and synthetic zero points defined by Holtzman et al. (1995a, 1995b) for the WFPC2 photometric system. In the WFPC2 system, Vega has $m \approx 0$ through all broad- and medium-band WFPC2 filters. This system differs significantly from the standard STScI magnitude system (STMAG), in which an object with a constant-F_λ spectrum and $m = 0$ has a monochromatic flux of $F_\lambda = 3.63 \times 10^{-9}$ ergs cm^{-2} s^{-1} Å^{-1}.

3. RESULTS

Figure 1 shows $9.''1 \times 13.''7$ sections of the long-exposure F1042M, F814W, and F675W images of the Gl 229 system obtained on UT 1995 November 17. The logarithms of the pixel intensities are displayed to reduce image contrast. The fields have been rotated counterclockwise by 13° so that north is up and east is to the left. Evident in the images are the diffraction spikes caused by the *HST* and PC secondary-mirror spiders and the charge overflow from the saturated pixels near Gl 229A. The source located to the south-southeast of Gl 229A is the same object identified by N95 as the brown dwarf companion Gl 229B. The image sections have been normalized to the same brightness at a distance of 30 pixels (1.″4) from Gl 229A to emphasize the redness of Gl 229B at optical wavelengths. Despite the logarithmic display, Gl 229B is barely detectable in the F675W image.

3.1. *Photometry of Gl 229B*

Table 1 lists the fluxes and WFPC2 magnitudes for Gl 229AB in the F1042M, F814W, and F675W bandpasses measured for each epoch. The equivalent STScI magnitudes are listed for sake of comparison. The values for Gl 229B were obtained using the average PSF-subtracted subimages described in § 2 and the photometric calibration technique of Holtzman et al. (1995a). The uncertainties in the fluxes represent the combined effects of read noise, photon noise, PSF subtraction error, flat-field inaccuracy (1% on small scales), and zero-point uncertainty ($\lesssim 2\%$). The measured fluxes of Gl 229B through F1042M and F814W are consistent with the Gunn *z* and *i* measurements reported by N95 (and tabulated by M96), and are up to 5 times more certain. The detection of Gl 229B through F675W is the first ever reported at *R*-band wavelengths (N95; Schultz et al. 1998). The WFPC2 colors of Gl 229B measured from the first-epoch images are $m_{675} - m_{814} = 3.84 \pm 0.24$ and $m_{814} - m_{1042} = 4.39 \pm 0.06$.

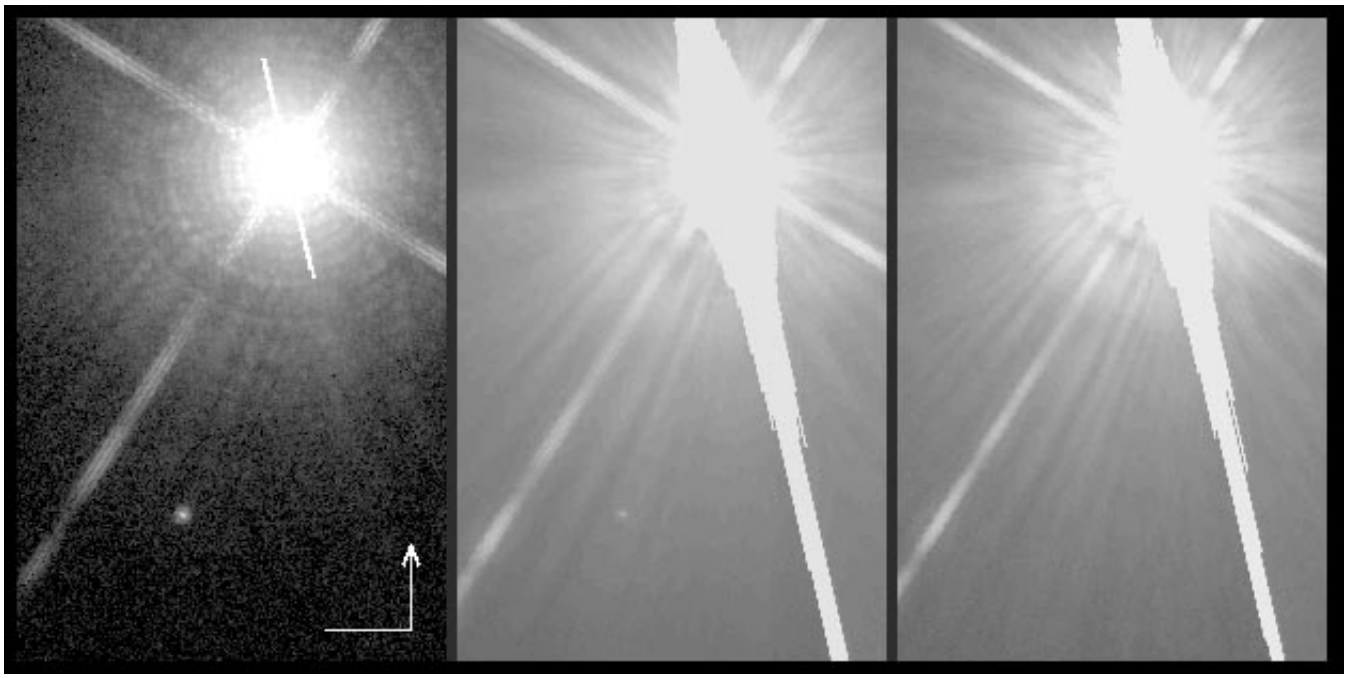

FIG. 1.—Images of Gliese 229AB obtained on UT 1995 November 17 using the *HST* Planetary Camera. The panels are 9″.1 × 13″.7 sections of two combined 300 s exposures through F1042M (*left*), two combined 400 s exposures through F814W (*middle*), and one 500 s exposure through F675W (*right*). The logarithms of the pixel intensities are presented to reduce image contrast. The fields have been rotated counterclockwise by 13° so that north is up (indicated by the arrow) and east is left. Gl 229B is located 7″.761 from Gl229A at a position angle of 163°.55. The panels have been normalized to a common brightness 30 pixels (1″.4) from Gl 229A to emphasize the redness of Gl 229B at optical wavelengths. Although barely detectable in the bottom panel, Gl 229B is imaged through F675W with S/N = 5.

The F1042M fluxes measured for Gl 229AB are invariant from epoch to epoch. However, the F814W fluxes of Gl 229B measured in epochs 1 and 2 do not agree within the computed uncertainties. The lack of temporal and chromatic correlation between these measurements discourages the notion that Gl 229B is photometrically variable. The discrepancy is more likely attributable to the photometric performance of WFPC2 and the flux calibration of the data. Holtzman et al. (1995a, 1995b) reported that the WFPC2 CCDs have substandard charge transfer efficiency, which may cause absolute photometric errors as large as 4% depending on the brightness and location of the source and background signal. Moreover, small changes in the detection efficiency of the PC can occur in the days or weeks between the calibration and science observations. For example, the fluxes measured from the images calibrated shortly after each observation by the STScI data pipeline (Leitherer et al. 1995) differed by 3%–4% from those measured from images recalibrated later using better suited calibration data. Although these instrumental and calibration errors cannot be precisely quantified, their combined uncertainty probably exceeds the 1% required to bring the discrepant F814W fluxes into accord.

3.2. *Relative Astrometry of Gl 229B*

The motive for choosing three observational epochs spaced 6 months apart was to compute explicitly and independently the proper motion and parallax of Gl 229B. With

TABLE 1

WFPC2 PHOTOMETRY OF GLIESE 229AB

FILTER	EXPOSURE (s)	DATE (UT)	F_λ (ergs cm^{-2} s^{-1} Å^{-1})[b]	F_ν (Jy)[b]	MAGNITUDE[a] STMAG	WFPC2	Error[b]	S/N[c]
Gl 229A:								
F1042M.....	1.6	1995 Nov 17	$(3.844 \pm 0.086) \times 10^{-12}$	13.38 ± 0.30	7.438	5.481	±0.024	862
		1996 May 26	$(3.851 \pm 0.086) \times 10^{-12}$	13.40 ± 0.30	7.436	5.479	±0.024	607
		1996 Nov 11	$(3.869 \pm 0.087) \times 10^{-12}$	13.47 ± 0.30	7.431	5.474	±0.024	862
Gl 229B:								
F1042M.....	300	1995 Nov 17	$(5.08 \pm 0.18) \times 10^{-16}$	$(1.77 \pm 0.06) \times 10^{-3}$	17.14	15.18	±0.04	35
		1996 May 26	$(5.19 \pm 0.15) \times 10^{-16}$	$(1.80 \pm 0.05) \times 10^{-3}$	17.11	15.16	±0.03	56
		1996 Nov 11	$(5.09 \pm 0.16) \times 10^{-16}$	$(1.77 \pm 0.06) \times 10^{-3}$	17.13	15.18	±0.03	45
F814W	400	1995 Nov 17	$(1.77 \pm 0.06) \times 10^{-17}$	$(3.76 \pm 0.13) \times 10^{-5}$	20.78	19.57	±0.04	37
		1996 May 26	$(1.90 \pm 0.05) \times 10^{-17}$	$(4.04 \pm 0.10) \times 10^{-5}$	20.70	19.49	±0.03	68
F675W	500	1995 Nov 17	$(8.57 \pm 1.71) \times 10^{-19}$	$(1.28 \pm 0.26) \times 10^{-6}$	24.07	23.41	$^{+0.24}_{-0.20}$	5

[a] Magnitudes are based on synthetic zero points given by Holtzman et al. 1995a for the STScI and WFPC2 photometric systems. Zero points are defined for a 0″.5 radius aperture.

[b] Uncertainties include read noise, photon noise, background subtraction error, calibration accuracy, and instrumental effects (see § 3.1).

[c] Based on read noise, photon noise, and background subtraction error only.

these parameters, the brown dwarf's bolometric luminosity and companionship with Gl 229A could be verified. This task required the presence of distant background stars in the PC FOV against which the motion of Gl 229B could be measured. No such stars appeared in the 300 s images through F1042M, but five faint (>20 mag) stars did appear in the 400 s images through F814W. Unfortunately, because of a miscommunication during observation planning, no F814W images were recorded during the third epoch. Consequently, independent derivations of Gl 229B's proper motion and parallax were unobtainable. Nevertheless, astrometric measurements relative to Gl 229A were obtainable and permitted a reliable assessment of Gl 229B's nature as a binary companion.

To determine accurately the position of Gl 229B relative to Gl 229A, the image centroids of each were computed using the 1.6 and 300 s exposures through F1042M. Because the signal-to-noise ratio (S/N) of each source's image is large (see Table 1), the accuracy of the centroid as a position estimator is limited not by photon noise but by telescope pointing, background subtraction, image distortion, and the accuracy of the centroid algorithm itself. Variations of Gl 229A's centroid measured from the individual 1.6 s images showed that the rms error of the interexposure pointing offsets was at most 0.03 pixels along each axis of the PC. Thus, the centroids measured from the combined 1.6 and 300 s images were unaffected by pointing error and jitter. Measurements of Gl 229B's centroid from the final background-subtracted subimages described in § 2 varied by $\lesssim 0.01$ pixels (rms), indicating an insensitivity to the order of the bivariate polynomial fit. Gilmozzi et al. (1995) characterized the geometric image distortion caused by the WFPC2 optics and derived equations of transformation between measured image centroids and orthogonal coordinate systems for each WFPC2 camera. They computed an rms error between actual and transformed coordinates of ~ 0.11 PC pixels. Monet (1992) estimates the accuracy of the image centroid algorithm to be ~ 0.1 pixels. Combined in quadrature, these uncertainties amount to an actual image-center error of ~ 0.16 PC pixels.

Any measured changes in the position angle of Gl 229AB between epochs are limited in accuracy by the uncertainty of *HST*'s roll-angle offset between visits. This uncertainty may be quantified by examining the positions of fixed background stars in the WFPC2 images. The five background stars appearing in the F814W PC images are useful for determining the angular offset of the PC between epochs 1 and 2. Although no background stars appeared in the F1042M PC images, 51 stars were imaged by the three WFCs in epochs 1 and 3. These 51 stars may be used to determine the angular offset of the PC between epochs 1 and 3 *only if* the offsets of the PC and WFCs are consistently identical. If so, the 25 stars appearing in that 20% of the WFC FOV imaged in both epochs 1 and 2 also may be used to improve the offset statistics generated by the five stars in the PC images.

To compute the roll-angle offsets between epochs, the position angles of all pairs of background stars imaged in each camera were computed from their distortion-corrected centroids (Gilmozzi et al. 1995) and then differenced from the position angles of the same star pairs imaged in different epochs. The differences were then weighted by the product of the fluxes of the star pairs and averaged to produce a mean angular offset between epochs for each camera. The resultant offsets are shown in Table 2. The uncertainties reflect the rms deviation of the individual offsets measured for the star pairs imaged in the respective cameras. (Note that the star pairs imaged by WF2 during epochs 1 and 2 appeared in WF4 during epochs 2 and 1, respectively. Stars imaged by WF3 in epochs 1 and 2 were not reimaged in epochs 2 and 1, respectively.) The resultant offsets for epochs 1 and 2 are the same, within the uncertainties, for the PC and the WFCs. Similar agreement is seen among the resultant offsets measured for epochs 1 and 3 using the three WFCs, so the average of these offsets may be confidently applied to the third-epoch PC images.

TABLE 2

ROLL-ANGLE OFFSETS BETWEEN EPOCHS

CAMERA[a]	FILTER	ROLL-ANGLE OFFSET (deg)	
		Epoch 2–Epoch 1	Epoch 3–Epoch 1
PC1.....	F814W	179.86 ± 0.02	...
WF2.....	F814W	179.87 ± 0.03	...
	F1042M	179.93 ± 0.06	359.86 ± 0.03
WF3.....	F1042M	...	359.84 ± 0.03
WF4.....	F814W	179.88 ± 0.06	...
	F1042M	...	359.87 ± 0.03
Average...		179.88 ± 0.02	359.86 ± 0.02

[a] Camera in which star pairs were imaged during epoch 1.

Using an image scale of 0.″04554 pixel^{-1} for the PC (Holtzman et al. 1995b), a first-epoch *HST* roll angle of 328.°00 $\pm$ 0.°07 (determined from the PA_V3 image-header keyword and a guide star position error of 1″), and the average roll-angle offsets from Table 2, we find that Gl 229B lay at the following separations and position angles from Gl 229A:

1995 November 17: 7.″761 $\pm$ 0.″007 at 163.°55 $\pm$ 0.°10 ,

1996 May 26: 7.″720 $\pm$ 0.″007 at 163.°69 $\pm$ 0.°10 ,

1996 November 11: 7.″674 $\pm$ 0.″007 at 163.°91 $\pm$ 0.°10 .

The change in the relative position of Gl 229B between epochs 1 and 3 (0.″100 $\pm$ 0.″013) is ~ 50 σ less than the annual proper motion of Gl 229A (0.″727 $\pm$ 0.″001 yr^{-1}; ESA 1997). Since the parallactic motion of both objects over 0.98 yr is nearly zero, we concur with N95 that Gl 229A and B exhibit common proper motion. Barring the unlikely scenario that the pair are comoving but not gravitationally bound, we conclude that the monotonic motion of Gl 229B relative to Gl 229A tabulated above is orbital in nature.

3.3. *Search for Fainter Companions*

The large S/N of the F1042M and F814W images of Gl 229B demonstrates the usefulness of WFPC2 for seeking faint companions to nearby stars. Schroeder & Golimowski (1996) assessed the PC's ability to detect such companions and formulated an algorithm that systematically identifies point sources embedded in the PC's complex PSF. They determined that this algorithm can locate a faint source anywhere within the circumstellar field provided that the source's brightness is at least 10 σ above the local background. We applied this search algorithm to the PC images of Gl 229AB to identify any fainter companions in the system and to establish an upper limit to the brightness of any undetected companions.

Because the same field was imaged by the PC in all three epochs, the search algorithm was applied to the first-epoch

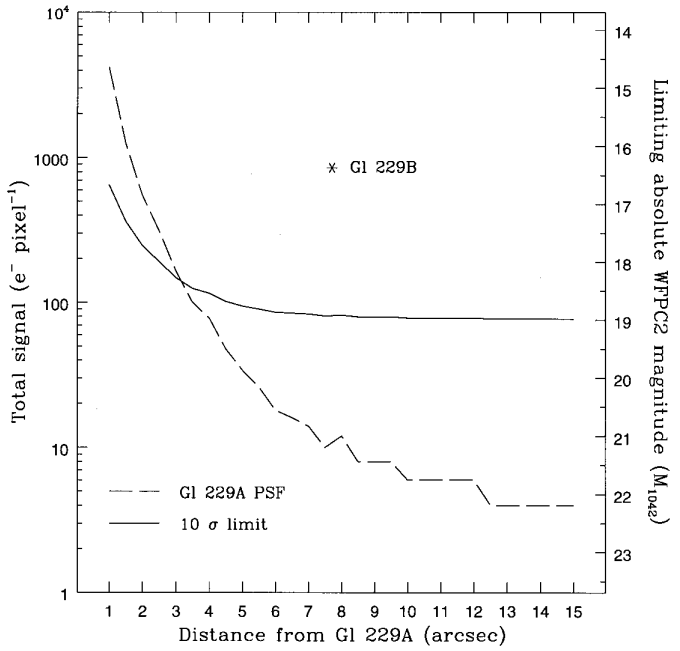

FIG. 2a

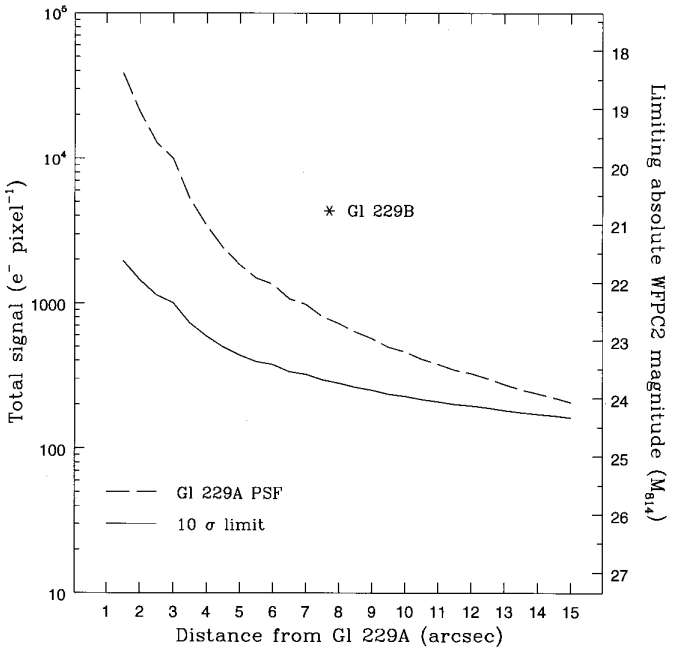

FIG. 2b

FIG. 2.—Signal and absolute magnitude detection limits for faint companions to Gl 229A imaged in the PC through (*a*) F1042M, and (*b*) F814W. The dashed curves show the azimuthally averaged image profiles of Gl 229A through each bandpass. The solid curves trace the detection limits for point sources having 4 pixels equal to 10 σ above the local background. The location and brightness of Gl 229B in each bandpass is plotted for reference.

F1042M and F814W images only. The search space was centered on Gl 229A and spanned the entire PC FOV except for those regions vignetted by the shadow of the WFPC2 pyramid (Burrows et al. 1995) or saturated by the excess charge from Gl 229A's image. Because the excess charge flows predominantly along the columns of pixels, the inner radial limit of the search varied with azimuth. The minimum search radii (oriented perpendicular to the charge overflow) were $\sim$0.″25 for the 300 s F1042M image and $\sim$1.″25 for the 400 s F814W image. The 5 s F814W image was also examined to provide search coverage of the region 0.″25–1.″25 from Gl 229A in that bandpass. The dashed curves in Figures 2*a* and 2*b* show the azimuthally averaged profiles of Gl 229A from the long-exposure F1042M and

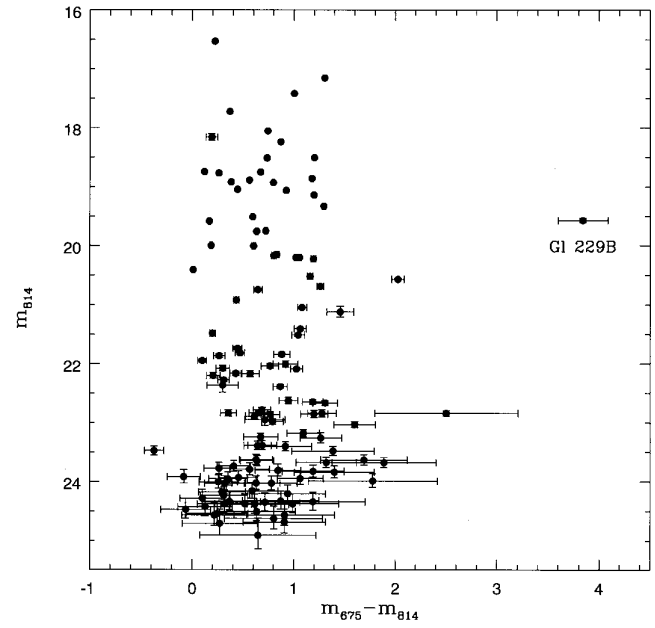

FIG. 3a

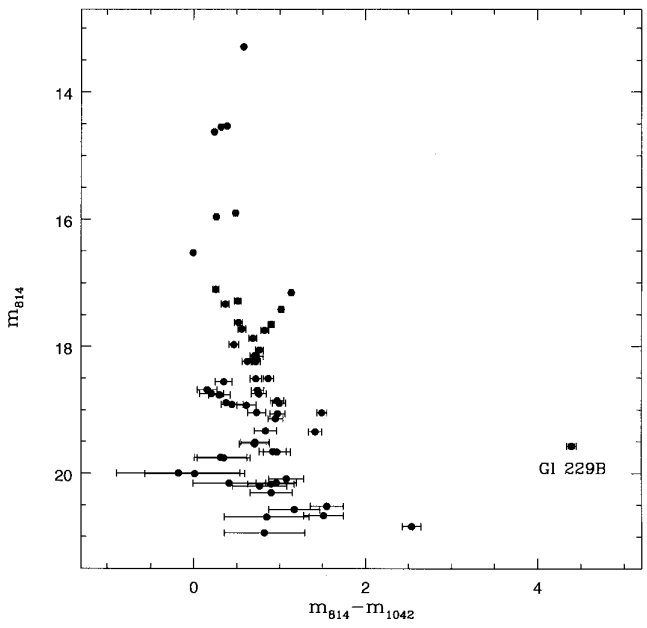

FIG. 3b

FIG. 3.—Color-magnitude diagrams of all point sources identified in the WFPC2 FOV during any two epochs. (*a*) Plot of m_{814} vs. $m_{675} - m_{814}$. (*b*) Plot of m_{814} vs. $m_{814} - m_{1042}$. Gl 229B is plotted for reference. No other source is sufficiently red to be considered a very low mass companion candidate. Moreover, none of the other sources exhibit common proper motion with Gl 229AB.

F814W images, respectively. The profiles were sampled over 5×5 pixel arrays in radial steps of 0.″5 and azimuthal intervals of 30°. Care was taken to avoid the diffraction spikes, charge overflow, and Gl 229B. The solid curves trace the detection limits for point sources having 4 pixels equal to 10 σ above the local background. In each figure, the location and brightness of Gl 229B is plotted as a point of reference. The figures demonstrate that F1042M is the better bandpass for seeking Gl 229B–like objects within 4″ of Gl 229A, while F814W is more suitable for searching beyond this angular distance.

The search algorithm identified six astronomical sources (excluding Gl 229B) in the F814W image and none in the F1042M image. The six sources in the F814W image consisted of five faint ($20.5 < m_{814} < 22.5$) stars (one of which was binary) and one bright ($m_{814} \approx 18$) galaxy. These six sources also appeared in the F675W image; none were redder than $m_{675} - m_{814} = 1.5$. None of the sources exhibited proper motion greater than 0.″02 (0.5 pixels) between epochs 1 and 2, so all were deemed to be distant background objects.

Because the background signal in the WFC images was mostly devoid of scattered light from Gl 229A, visual inspection alone was sufficient for identifying sources with S/N $\gtrsim$ 5. We computed the fluxes and distortion-free centroids of all WFC sources with F1042M and F814W fluxes brighter than S/N = 5 (i.e., $m_{1042} < 19.2$ and $m_{814} < 24.7$) that appeared in at least two epochs or bandpasses. These selection criteria permitted identification of widely separated companion candidates from their colors or proper motions. We identified 174 sources, of which 159 are point-like (presumably stars) and 15 are galaxies. Figures 3*a* and 3*b* show the color-magnitude diagrams of all the point sources identified in the WFPC2 FOV during any two epochs. The distribution of colors in each figure is consistent with interstellar reddening at a Galactic latitude of −18°. No source is sufficiently red to be considered a very low mass companion candidate. Moreover, none of the WFC sources exhibit any significant proper motion.

In summary, we detected no other potential companions to Gl 229A brighter than (1) the 10 σ limits depicted in Figure 2 for the PC images and (2) $M_{1042} = 20.4$ or $M_{814} = 25.9$ in the WFC images.

4. DISCUSSION

Using a parallax of 0.″17319 ± 0.″00112 for Gl 229A (ESA 1997) and the first-epoch images, we compute for Gl 229B absolute WFPC2 magnitudes of $M_{1042} = 16.37 \pm 0.04$, $M_{814} = 20.76 \pm 0.04$, and $M_{675} = 24.60^{+0.24}_{-0.20}$. Thus, Gl 229B is the least luminous object beyond our solar system ever imaged at optical wavelengths. The broadband flux ratios measured from the same images are $f_{1042}/f_{814} = 28.7$ and $f_{814}/f_{675} = 20.7$. Since the interval between the pivot wavelengths of F814W and F1042M is about 1.75 times that between F675W and F814W, the average flux from Gl 229B in these bandpasses increases ∼28% more rapidly between F675W and F814W than it does between F814W and F1042M.

Tsuji et al. (1996) and M96 have shown that the broadband fluxes from 0.8 to 10 μm reported by M96 are well fitted by model spectra of dust-free, brown dwarf photospheres with $T_{\rm eff} = 900$ and 1000 K. Tsuji has kindly provided us with two sets of his revised dust-free models for $T_{\rm eff} = 900$ and 1000 K. The sets are distinguished by the inclusion (model A) or exclusion (model C) of opacity from TiO and VO. Both sets of models include some transitions of H_2O and CH_4. We compare our WFPC2 measurements with Tsuji's model spectra in Figure 4. Both model C spectra match the measured F1042M flux well, but they severely overestimate the fluxes observed through F675W and F814W. Although absorption by TiO and VO is absent from the observed optical spectrum of Gl 229B (Oppenheimer 1998; Schultz et al. 1998; Oppenheimer et al. 1998), the model A spectra are significantly better matches to the F675W and F814W fluxes. Schultz et al. (1998) noted a similar overestimation of Gl 229B's optical flux in the model spectra of Allard et al. They surmised that the emergent flux shortward of 0.8 μm is strongly absorbed by dust grains suspended in the photosphere. Oppenheimer et al. (1998), however, have reported that the near-infrared spectrum of Gl 229B cannot be reproduced by any of the dusty-photosphere models of Tsuji et al. (1996). Because these models consider the effects of only the most abundant species of dust, it remains to be seen whether this dilemma can be resolved by the inclusion of condensates from less abundant refractory elements.

Although the spectral energy distribution of Gl 229B has been studied extensively in the last 2 years, the question concerning Gl 229B's formation as a binary or a planetary companion remains unanswered. Boss (1996) has suggested that orbital eccentricity may resolve this question, since binary stars usually have elliptical orbits (Duquennoy & Mayor 1991) and planets form with nearly circular orbits. The 1 year span of our observations is insufficient for com-

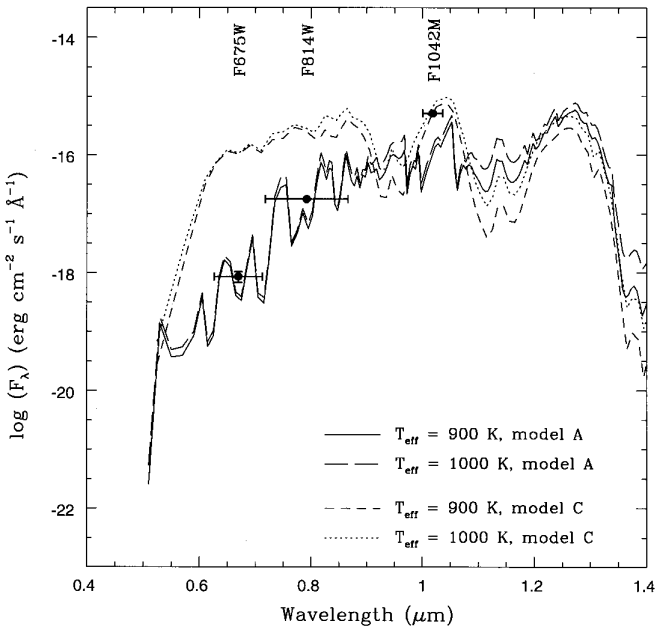

FIG. 4.—Comparison of measured WFPC2 broadband fluxes with models of dust-free, brown dwarf photospheres by Tsuji. Optical spectra are shown for brown dwarfs with solar metallicity, log $g = 5$, and $T_{\rm eff} =$ 900 and 1000 K at a distance of 5.774 pc. The spectra are grouped according to the inclusion (model A) or the exclusion (model C) of opacity from TiO and VO. (Neither molecule is observed in the actual optical spectrum of Gl 229B.) All models include some transitions of H_2O and CH_4. The model C spectra match the measured F1042M flux well, but severely overestimate the observed fluxes through F675W and F814W. These fluxes are betted matched by the model A spectra, which indicates that a strong source of optical continuum opacity exists in the photosphere of Gl 229B.

puting Gl 229B's orbit, but its eccentricity can be constrained from our astrometry and Kepler's laws. The semimajor axis, a, of a Keplerian orbit is

$$a = \left(\frac{2}{r} - \frac{v^2}{\mu}\right)^{-1}, \quad (1)$$

where $r = |\boldsymbol{r}(t)|$ and $v = |\boldsymbol{v}(t)|$ are the separation and velocity of the orbiting body at time t. The quantity μ equals $G(m_1 + m_2)$, where G is the gravitational constant and m_1 and m_2 are the component masses. For bound orbits, $a \geq 0$. The eccentricity, e, of a bound orbit is

$$e = \sqrt{\left(1 - \frac{r}{a}\right)^2 + \left(\frac{u}{na^2}\right)^2}, \quad (2)$$

where $u = \boldsymbol{r} \cdot \boldsymbol{v}$, and $n = (\mu/a^3)^{1/2}$ (Danby 1988).

Equations (1) and (2) cannot be solved uniquely without knowing Gl 229B's motion along the line of sight, but a and e can be constrained from the observed motion in the plane of the sky. Gl 229B's motion between epochs 1 and 3 was $0''.100 \pm 0''.013$, of which $-0''.087 \pm 0''.010$ (1.91 ± 0.23 pixels) was radial motion and $+0''.049 \pm 0''.019$ (1.07 ± 0.42 pixels) was azimuthal motion. Assuming a mass of 0.57 $M_\odot$ for Gl 229A (Henry & McCarthy 1993), we have computed lower limits to the kinetic (T) and potential (U) energies of Gl 229B from its projected position and velocity between these epochs. We find that $T_{\rm min}/U_{\rm min} \approx -0.34$, which strongly supports (though does not prove) a bound orbit. Figures 5*a* and 5*b* depict the loci of a and e, respectively, for such orbits, based on Gl 229B's average position and velocity between epochs 1 and 3, varying values of Gl 229B's line-of-sight position and velocity, and an estimated mass for Gl 229B of 0.045 $M_\odot$. From these parameters, we compute $a \gtrsim 32$ AU, a period $P = (4\pi^2 a^3/\mu)^{1/2} \gtrsim 236$ yr, and $e \gtrsim 0.25$. (For the 6 month intervals between epochs 1 and 2 and epochs 2 and 3, $e \gtrsim 0.07$ and 0.45, respectively.) Although this eccentricity may imply a binary rather than planetary origin for Gl 229B, a verdict based solely upon the small sample statistics of known planetary orbits is questionable at best.

The theory and observation of brown dwarf atmospheres are in their adolescence. At this time, we cannot accurately predict the F1042M and F814W fluxes of brown dwarfs older or less massive than Gl 229B. Therefore, we cannot with certainty interpret the limiting magnitudes of our search for fainter companions in terms of age or mass limits. Rough estimates are possible, however, if assumptions are made about the behavior of the optical spectra of older or less massive brown dwarfs. Burrows et al. (1997) have made the first theoretical predictions of the infrared colors and absolute magnitudes of brown dwarfs with $T_{\rm eff} \lesssim 1300$ K. They present an M_J versus $J-K$ diagram showing the theoretical isochrones of brown dwarfs with ages 0.5, 1, and 5 Gyr (their Fig. 20). If we assume that M_{1042} scales proportionally to M_J (not an unreasonable assumption, given their model spectra), then the asymptotic limit of the 10 σ detection curve in Figure 2*a* corresponds approximately to mass detection limits of 10, 15, and 33 $M_{\rm Jup}$ for brown dwarfs of age 0.5, 1, and 5 Gyr, respectively. Likewise, the mass detection limits corresponding to $M_{1042} = 20.4$ for the WFCs are about 7, 10, and 23 $M_{\rm Jup}$ for brown dwarfs of age 0.5, 1, and 5 Gyr, respectively. Although the F814W magnitude limits are deeper than those for F1042M, the F814W flux from brown dwarfs drops with decreasing $T_{\rm eff}$ more rapidly than the F1042M flux. Consequently, F814W may be less sensitive than F1042M to old or low-mass brown dwarfs.

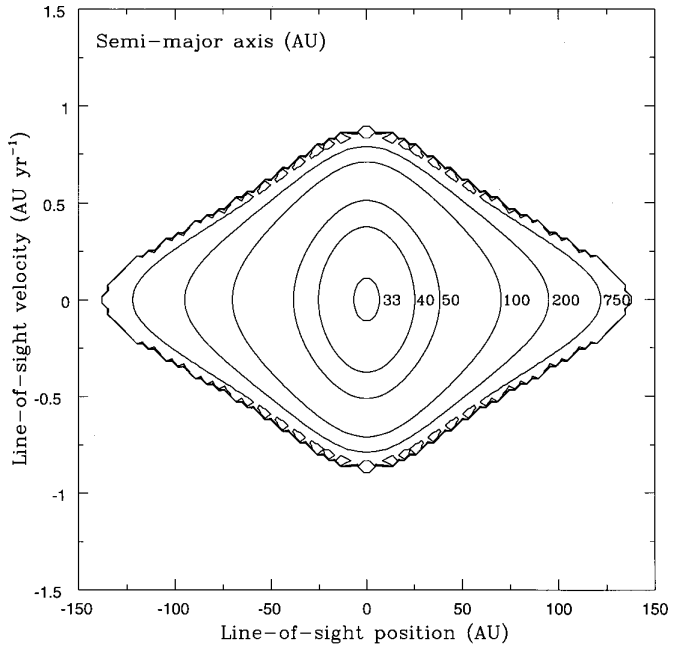

FIG. 5*a*

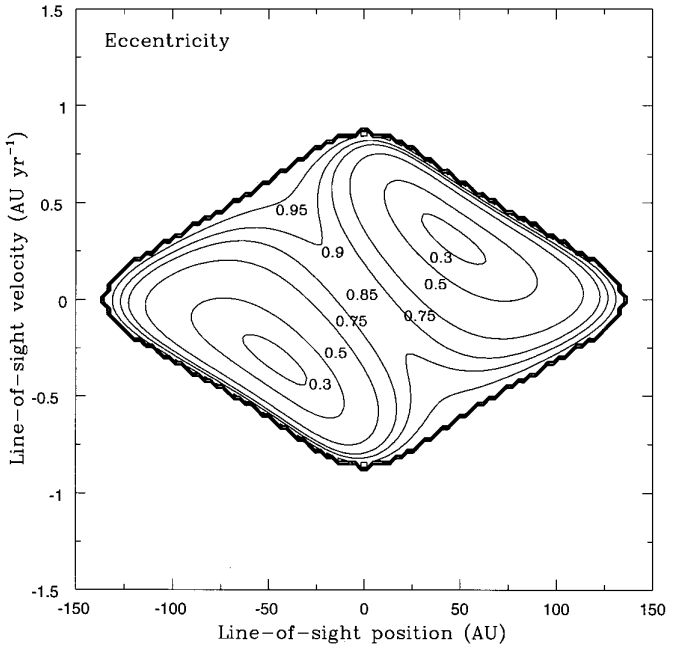

FIG. 5*b*

FIG. 5.—Loci of (*a*) semimajor axes and (*b*) eccentricities consistent with bound Keplerian orbits and the observed motion of Gl 229B between epochs 1 and 3. The parameters are shown as functions of the line-of-sight position and velocity of Gl 229B relative to the the plane of the sky. The heavy contours reflect the boundaries between bound and unbound orbits. We compute $a \gtrsim 32$ AU, $e \gtrsim 0.25$, and $P \gtrsim 236$ yr for Gl 229B, assuming masses of 0.57 and 0.045 $M_\odot$ for Gl 229A and B, respectively.

The authors thank Robert Williams of STScI for the use of his Director's discretionary time. We also thank Takashi Tsuji for providing us with his revised model spectra. Finally, we thank the referee for many useful suggestions. Support for this work was provided by NASA through grants GO-06338.01-94A and GO-06338.02-94A from the Space Telescope Science Institute, which is operated by the Association of Universities for Research in Astronomy, Inc., under NASA contract NAS 5-26555.

REFERENCES

Allard, F., Hauschildt, P. H., Baraffe, I., & Chabrier, G. 1996, ApJ, 465, L123
Boss, A. P. 1996, Nature, 379, 397
Burrows, A., & Liebert, J. 1993, Rev. Mod. Phys., 65, 301
Burrows, A., et al. 1997, ApJ, 491, 856
Burrows, C. J., et al. 1995, Wide Field and Planetary Camera 2 Instrument Handbook (version 3.0; Baltimore: STScI)
Da Costa, G. S. 1992, in ASP Conf. Ser. 23, Astronomical CCD Observing and Reduction Techniques, ed. S. B. Howell (San Francisco: ASP), 90
Danby, J. M. A. 1988, Fundamentals of Celestial Mechanics (2d ed.; Richmond: Willman-Bell), 165
Duquennoy, A., & Mayor, M. 1991, A&A, 248, 485
ESA. 1997, The Hipparcos and Tycho Catalogues (ESA SP-1200) (Noordwijk: ESA)
Fegley, B., & Lodders, K. 1996, ApJ, 472, L37
Geballe, T. R., Kulkarni, S. R., Woodward, C. E., & Sloan, G. C. 1996, ApJ, 467, L101
Gilmozzi, R., Ewald, S., & Kinney, E. 1995, The Geometric Distortion Correction for the WFPC Cameras (WFPC2 ISR 95-02) (Baltimore: STScI)
Henry, T. J., & McCarthy, D. W. 1993, AJ, 106, 773
Holtzman, J. A., Burrows, C. J., Casertano, S., Hester, J. J., Trauger, J. T., Watson, A. M., & Worthey, G. 1995a, PASP, 107, 1065
Holtzman, J. A., et al. 1995b, PASP, 107, 156
Leitherer, C., et al. 1995, *HST* Data Handbook (version 2.0; Baltimore: STScI)
Marley, M. S., Saumon, D., Guillot, T., Freedman, R. S., Hubbard, W. B., Burrows, A., & Lunine, J. I. 1996, Science, 272, 1919
Matthews, K., Nakajima, T., Kulkarni, S. R., & Oppenheimer, B. R. 1996, AJ, 112, 1678 (M96)
Monet, D. G. 1992, in ASP Conf. Ser. 23, Astronomical CCD Observing and Reduction Techniques, ed. S. B. Howell (San Francisco: ASP), 221
Nakajima, T., Oppenheimer, B. R., Kulkarni, S. R., Golimowski, D. A., Matthews, K., & Durrance, S. T. 1995, Nature, 378, 463 (N95)
Noll, K. S., Geballe, T. R., & Marley, M. S. 1997, ApJ, 489, L87
Noll, K. S., Knacke, R. F., Geballe, T. R., & Tokunaga, A. T. 1988, ApJ, 324, 1210
Oppenheimer, B. R. 1998, in ASP Conf. Ser. 134, Brown Dwarfs and Extrasolar Planets, ed. R. Rebolo, E. L. Martín, & M. R. Zapatero Osorio (San Francisco: ASP), 196
Oppenheimer, B. R., Kulkarni, S. R., Matthews, K., & Nakajima, T. 1995, Science, 270, 1478
Oppenheimer, B. R., Kulkarni, S. R., Matthews, K., & van Kerkwijk, M. H. 1998, ApJ, submitted (astro-ph/9802299)
Schroeder, D. J., & Golimowski, D. A. 1996, PASP, 108, 510
Schultz, A. B., et al. 1998, ApJ, 492, L181
Tsuji, T., & Ohnaka, K. 1995, in Elementary Processes in Dense Plasmas, ed. S. Ichimaru & S. Ogata (Reading: Addison-Wesley), 193
Tsuji, T., Ohnaka, K., Aoki, W., & Nakajima, T. 1996, A&A, 308, L29